Investigation of the vanadium L_{23}-edge x-ray absorption spectrum of $SrVO_3$ using configuration interaction calculations: Multiplet, valence, and crystal-field effects

M. Wu, J.-C. Zheng,* and H.-Q. Wang†

Fujian Provincial Key Laboratory of Semiconductors and Applications, Collaborative Innovation Center for Optoelectronic Semiconductors and Efficient Devices, Department of Physics, Xiamen University, Xiamen 361005, People's Republic of China

(Received 17 April 2018; published 25 June 2018)

Configuration interaction cluster calculations have been performed to investigate the electronic structure of orthorhombic distorted $SrVO_3$ compound, where a considerable tetragonal crystal-field splitting of larger than 180 meV for t_{2g} orbital levels is suggested for the good consistence between the simulated and the experimental spectral line shape. This supports the crystal-field splitting scenario for the metal-insulator transition mechanism. We further calculate V L_{23}-edge absorption spectra of vanadium oxides with similar VO_6 octahedral environment for formal d electrons varying from $3d^0$ to $3d^3$, where we obtain energy parameters representing the local ground-state properties and provide the theoretical guidance for identifying the chemical valence and the crystal-field strength of a particular vanadium oxide. Our simulated polarization-dependent spectra at different tetragonal crystal-field values reveal a nonlinear orbital-lattice interaction. The orbital polarization P reflecting the electron occupations in different d_{xy} and $d_{xz(yz)}$ orbital symmetries shows strong sensitivity to small tetragonal crystal field, indicating the strongly correlated electron effect and further addressing the efficiency of strain engineering in functional SVO-based thin films and heterostructures.

DOI: 10.1103/PhysRevB.97.245138

I. INTRODUCTION

Vanadium-based strongly correlated systems show both challenges for understanding the interplay of different degrees of freedom that drives the metal-insulator transition (MIT) and prospects for applications into next generation optoelectronic devices [1]. $SrVO_3$ (SVO) compound, for instance, exhibits potential applications as a bottom electrode with structural and chemical compatible with other functional oxides [2] and as a transparent conductor in the visible spectral range [3]. SVO compound has an ideal cubic perovskite structure with lattice constant of 3.843 Å and the V^{4+} cation adopts a $3d^1$ (t_{2g}^1) electronic configuration, which is often used as a prototypical example to test density functional theory plus dynamical mean-field theory (DFT+DMFT) calculations [4–6]. Bulk SVO is regarded as a correlated metal due to its anomalous effective-mass enhancement [7,8] and kick in the band dispersion [9]. Beneficial from the tremendous progress in the thin-film deposition techniques, SVO thin films have also been investigated showing interesting emerged electronic states. In particular, *in situ* angle-resolved photoemission experiments yield evidence of metallic quantum well states for SVO film with thickness less than ∼10 monolayers [10–12]. More interestingly, SVO ultrathin films undergo MIT below a critical film thickness, e.g., ∼2−3 monolayers for SVO deposited on $SrTiO_3$ substrate [10], and ∼17 monolayers for SVO deposited on $(LaAlO_3)_{0.3}(Sr_2AlTaO_6)_{0.7}$ substrate [13]. However, the underlying mechanisms for MIT are still under debate. The observed MIT has been attributed to the reduction of bandwidth based on the *in situ* photoemission spectroscopy measurement and were supported by the DMFT calculations using the single-band Hubbard model [10]. In contrast, Zhong *et al.* proposed the physical origin of the MIT as the lift of orbital degeneracy in response to the crystal-field effect based on DFT+DMFT calculations recently [14]. Recent experiments based on detailed x-ray spectroscopical studies have shown that an orthorhombic distortion of otherwise cubic SVO yields an insulator [15]. It is highly desirable to settle the controversies from a different approach which will be addressed by configuration interaction (CI) cluster calculations using the experimental V L_{23}-edge absorption spectrum of orthorhombic SVO compound as fingerprint.

The MIT, on the other hand, is found to be strongly affected by the chemical valence state in vanadium oxides due to their complex phases and available multivalence states [16–18]. Besides the typical mechanism such as the electron-electron interaction and electron-lattice interaction as the driving force for the MIT [19], various mechanisms have been proposed for mixed-valence oxides, e.g., the charge ordering proposed in interpreting the Verwey transition of mixed Fe^{2+} and Fe^{3+} magnetite [20]; the stripe-type charge ordering of coexisted Ni^{2+} and Ni^{3+} in $La_{2-x}Sr_xNiO_4$ compound [21]; the charge order between V^{4+} and V^{5+} in NaV_2O_5 compound [22] and between V^{2+} and V^{3+} in $BaV_{10}O_{15}$ [23], etc. Understanding and precise controlling of the targeted chemical valence is vital for both device application and fundamental research. Therefore, we perform CI based spectroscopy studies of different vanadium valence states, aiming for offering references for experimental synthesis as well as understanding the extraordinarily important MIT in correlated systems and the technical application utilizing the MIT.

*jczheng@xmu.edu.cn
†hqwang@xmu.edu.cn

In this paper, by using element-, local valence-, and orbital-sensitive L_{23}-edge x-ray absorption spectra as fingerprints, we perform configuration interaction (CI) based cluster calculations for VO_6 octahedra with different formal d electrons. In Sec. II A, we focus on the exploring of the multiplet structures of SVO compound with a distorted orthorhombic crystal structure. In Sec. II B, we present the comparison between theoretical and experimental spectra of vanadium oxides with different chemical valence states, which is valuable for compound synthesizing with targeted valence state and for understanding the physical mechanism. In Sec. II C, we present the photon polarization dependent absorption spectra with different tetragonal crystal fields for SVO compound. The quantity orbital polarization P is defined to evaluate the detailed orbital occupancies which can be used for a direct comparison with experimental results and other calculations. The polarization dependent study reveals the orbital-lattice coupling of the SVO system and provides guidance for strain engineering functional SVO-based thin films and heterostructures. Finally we present the conclusion.

II. RESULTS AND DISCUSSION

A. Metal-insulator transition mechanism

CI cluster calculation has been performed for a VO_6 cluster with $3d^1$ electronic configuration. Figure 1(a) shows the comparison between the experimental x-ray absorption spectrum of the orthorhombic SVO compound reproduced from Sharma *et al.* [15] and the simulated ones. The spectrum is composed of a L_3 and L_2 set of peaks owing to the spin-orbit coupling of the V $2p$ levels. We note that the multiplet structures in the absorption spectrum are different from VO_2 with the same nominal valences [24], indicating the strong sensitivity to small structural and electronic variations of the L_{23}-edge absorption spectrum. Our cluster calculation with optimized parameters can capture the features of the experimental spectrum well.

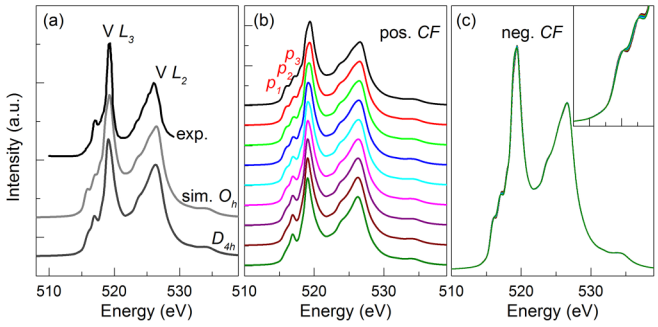

FIG. 1. (a) Comparison between the experimental x-ray absorption spectrum and the simulated spectra for the orthorhombic SVO compound. The V L_{23}-edge absorption spectra for $SV^{4+}O$ is reproduced from Sharma *et al.* [15]. Two simulated absorption spectra of respectively cubic O_h and tetragonal D_{4h} symmetries with $\Delta_{t2g} =$ 180 meV are shown for comparison. (b) Simulated absorption spectra for a VO_6 $3d^1$ cluster with different positive tetragonal crystal-field splitting values, i.e., 30, 60, 90, 120, 150, 180, 240, 300, 360 meV from top to bottom spectrum. Panel (c) shows the calculated spectra with different negative tetragonal crystal-field splitting values, i.e., −30, −60, −90, −120, −150, −180, −240 meV.

TABLE I. The best-fit energy parameters including the charge-transfer energy Δ, the on-site d-d Coulomb repulsion U_{dd}, and the d-p hybridization energy $pd\sigma$ for vanadium oxides of different valence states. Values from earlier CI based calculations are included for comparison.

Valence	d^n	Δ	U_{dd}	$pd\sigma$	Reference
V^{5+}	d^0	0.5	5.5	1.2	this work
V^{4+}	d^1	2.0	4.5	1.5	this work
V^{3+}	d^2	3.8	4.0	1.5	this work
V^{2+}	d^3	7.5	5.5	1.2	this work[a]
$V2^{5+}O_5$	d^0	0.5	5.5	2.7	Ref. [37]
$SV^{4+}O$ metallic	d^1	2.0	5.0	1.9	Ref. [25]
$CaV^{4+}O_3$ metallic	d^1	2.0	5.0	1.6	Ref. [25]
$V^{4+}O_2$	d^1	2.5	4.5		Ref. [24]
$V_2^{3+}O_3$	d^2	4.0	4.0	1.73	Ref. [37]
$LaV^{3+}O_3$	d^2	4.0	4.0	2.02	Ref. [37]
$LaV^{3+}O_3$	d^2	3.8	4.2	1.5	Ref. [25]
$YV^{3+}O_3$	d^2	3.8	4.2	1.5	Ref. [25]

[a]The energy parameters are taken from Saitoh *et al.* [38].

The parameters including the charge-transfer energy Δ, the on-site d-d Coulomb repulsion U_{dd}, and the d-p hybridization energy $pd\sigma$ are listed in Table I. We notice a clear reduction of the hybridization strength $pd\sigma$ from a direct comparison of the simulated energy parameters between insulating SVO and metallic SVO [25], suggesting the reduction of bandwidth crossing the MIT.

Figure 1(b) shows the simulated spectra for different positive tetragonal crystal-field values. The tetragonal crystal field is modelled by two additional energy parameters to represent further energy splitting, i.e., Δ_{t2g} and Δ_{eg}, denoting the energy splitting of t_{2g} levels [$\Delta_{t2g} = E(d_{yz,xz}) - E(d_{xy})$] and e_g levels [$\Delta_{eg} = E(d_{3z2-r2}) - E(d_{x2-y2})$], respectively. For a thoughtful understanding of the experimental absorption spectrum, Δ_{eg}, which effects the final-state properties, should be considered [26]. We use $\Delta_{eg} = 2\Delta_{t2g}$ in the first approximation, accounting for the anisotropic hybridization strength between the e_g-O p orbitals and the t_{2g}-O p orbitals. The simulated spectra at different tetragonal crystal fields and the cubic one show differences mainly in the prepeak line shape. We denote the three prepeaks as p_1, p_2, and p_3 in Fig. 1(b). The prepeak structure is fitted with three peaks of Lorentzian line shapes where the intensities of peak p_1 and p_3 show a slight reduction, while the peak p_2 shows a monotonous increase as Δ_{t2g} increases. To maintain good agreement with the spectral line shape of the orthorhombic SVO compound, the crystal field splitting is quite appreciable, i.e., Δ_{t2g} is larger than 180 meV. Figure 1(c) presents the simulated spectra for negative Δ_{t2g} and Δ_{eg} values, where we observe a smaller difference in the isotropic spectra with a reduction of peak p_2 intensity with Δ_{t2g} varying from −30 to −240 meV. This observation confirms the lower energy level of d_{xy} orbital for the ground-state properties and supports the recent tetragonal crystal-field scenario accounting for the MIT based on DFT+DMFT calculations [14].

B. Valence effects and crystal-field strength

The partially filled V-3d shell accompanied by a set of valence states form a number of vanadium oxides which differ widely in their physical and spectroscopic properties. Among them there are four single valence states, i.e., V^{5+}, V^{4+}, V^{3+}, and V^{2+}. The former has completely empty 3d states ($3d^0$) and is nonmagnetic, while the latter three are characterized by local spin and strong electronic correlations. Precise understanding of the chemical valence or oxidization states is highly valuable for not only fundamental research but also the engineering of functional oxides. Therefore, we perform CI cluster calculations to VO_6 octahedra with different formal electron numbers which offers a direct guidance for understanding the possible multivalence states of different vanadium oxides.

Figure 2 shows the simulated spectra for vanadium oxide with different valence states where we notice significant changes of the spectra line shapes besides the shift to high absorption energy with high valence. We note that due to the layer-type structure with weak interlayer bonding of the V_2O_5 compound, the high anisotropic coordination environment around vanadium should be taken into account to understand the multiplet structures, which however brings difficulties to understanding the V L_{23}-edge absorption spectrum using VO_6 octahedron based on CI cluster calculations [29]. We have not obtained the absorption spectra for VO_6 with V^{5+} and V^{2+} oxidation states with a local octahedral symmetry from the literature, to the best of our knowledge. The V L_{23}-edge absorption spectra for $V_2^{3+}O_3$ and $YV^{3+}O_3$ compounds are reproduced from Park *et al.* [27] and Benckiser *et al.* [28], respectively. Our simulated spectra show reasonably good agreement with experimentally measured absorption spectra, in terms of the capture of the overall line shapes and the characteristic peaks for V^{3+} and V^{4+}, as shown in Fig. 2. The best-fit energy parameters are listed in Table I.

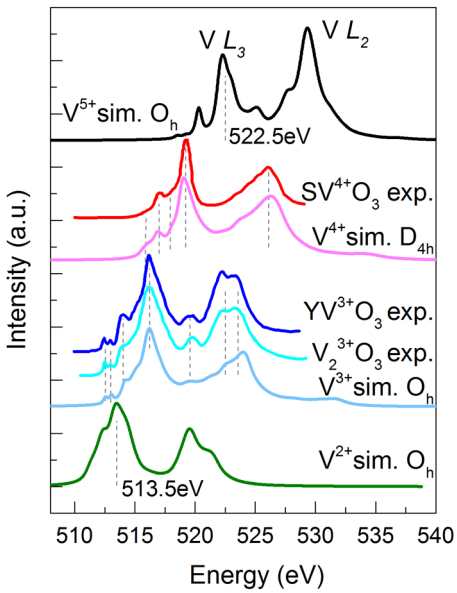

FIG. 2. Simulated spectra of different vanadium valence states and the comparison to experimental x-ray absorption spectra for V^{3+} and V^{4+}. The V L_{23}-edge absorption spectra for $V_2^{3+}O_3$ and $YV^{3+}O_3$ compounds are reproduced from Park *et al.* [27] and Benckiser *et al.* [28]. The first excitation peak of the simulated spectrum for V^{5+} and V^{2+} in a VO_6 octahedron is shifted to 522.5 and 513.5 eV, respectively, i.e., the same binding energy as V_2O_5 $2p_{3/2}$ [29] and VO $2p_{3/2}$ [30] obtained from x-ray photoelectron spectroscopy. All simulated spectra shown here are calculated at $10Dq = 1.0$ eV.

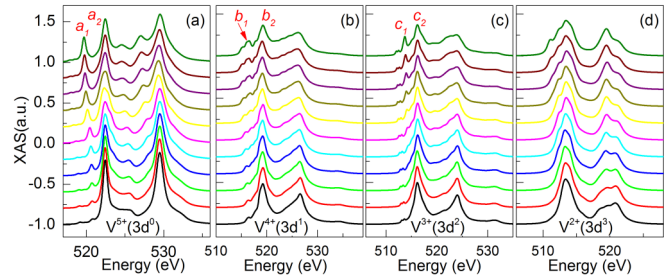

FIG. 3. Simulated isotropic absorption spectra for different $10Dq$ values for V^{5+} with $3d^0$ electronic configuration (a), V^{4+} with $3d^1$ electronic configuration (b), V^{3+} with $3d^2$ electronic configuration (c), and V^{2+} with $3d^3$ electronic configuration (d). In each panel, the crystal-field splitting $10Dq$ varies from 0 to 2 eV with an interval of 0.2 eV from the bottom to the top spectrum.

In comparison of the best-fit energy parameters obtained from CI calculations, a notable change is the decrease of the charge-transfer energy Δ going from V^{2+} to V^{5+}, which is due to the decrease of formal d electron number and a lowering of the 3d orbitals. We further calculate the spectra with different crystal-field strength $10Dq$ values while other parameters keep the optimized ones as shown in Table I. $10Dq$ reflects the charge potential of all other elements on the V site and the magnitude of $10Dq$ is related to the charge on the metal ion as well as the local environment, which in turn determines other physical properties, such as the low- or high-spin magnetic structure [31], the optical properties [32], etc. From a comparison of our simulated spectra as shown in Fig. 3 to an accurately measured absorption spectrum, one can obtain the $10Dq$ value, corresponding to the crystal-field strength.

However, since the read-off energy differences between t_{2g}-excited and e_g-excited peaks in L_3 and L_2 edges generally are not directly equal to the $10Dq$ values [26,33], we provide a quantitative analysis as shown in Fig. 4. Here, we focus on the excitation peak of L_3 edge, since the L_2 excitation peak is additionally broadened by Coster-Kronig decay [34]. The L_3 and L_2 absorption edges split as $10Dq$ increases. For VO_6 octahedron with $3d^0$, $3d^1$, and $3d^2$ electron configuration, we

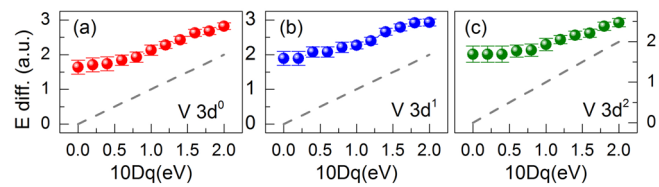

FIG. 4. The read-off energy difference between peak a_1 and a_2 (a), peaks b_1 and b_2 (b), and peaks c_1 and c_2 (c), as a function of the crystal-field strength $10Dq$ value. The grey dashed line denotes the same magnitude between the peak splitting and the $10Dq$.

use the energy difference between peaks a_1 and a_2, peaks b_1 and b_2, and peaks c_1 and c_2 to quantify the crystal-field splitting strength, as shown in Fig. 4. The real energy difference between the L_3 set of peaks is obviously deviated from the grey dashed line which represents the same magnitude between energy splitting and crystal field $10Dq$. The resolved energy splitting is larger than the $10Dq$ value, similar to the tendencies reported in the Ti^{4+} system [33], Mn^{2+} system [35], and Fe^{3+} system [36].

C. Crystal-field effects

Strain engineering has been proposed to tailor the electronic properties efficiently, e.g., the strengthening of ferroelectric properties [39,40], the enhancement of superconductivity transition temperature [41,42], and to produce exotic electronic and magnetic states [43,44]. Strain induced by lattice mismatch between thin film and substrate with different in-plane lattice constants generally lower the crystal symmetry from cubic O_h to tetragonal D_{4h}. Besides the isotropic spectra as discussed previously, for compounds with different orbital occupancies, the x-ray linear dichroism spectra with different linear-polarized photons are very valuable due to the advantage of providing formations of the oxidation states, orbital occupations, and local symmetry of the probed metal ion. We thus consider explicitly the above calculated VO_6 octahedron of the orthorhombic SVO compound with different photon polarizations, for the purpose of understanding the orbital-lattice interactions as well as quantifying the orbital occupancies for a direct comparison with experimental results and the theoretical values, e.g., the density of states obtained from DFT.

Figure 5(a) shows simulated spectra at different Δ_{t2g} and Δ_{eg} values with light polarization parallel ($E \parallel c$) and perpendicular ($E \perp c$) to the crystal c axis. The strict dipole selection rules allow a separation between two different types of orbitals, i.e., the d_{xy} orbital with orientation perpendicular to the crystal c axis and the d_{xz} and d_{yz} orbitals with orientations parallel to the crystal c axis. First, the simulated spectra show a strong polarization dependency attributed to different symmetries and occupations of the orbitals. The linear dichroic spectra are shown in Figs. 5(b) and 5(c), where the normalized difference shows a systematic increase in magnitude as the tetragonal crystal-field splitting increases. Due to the anisotropic symmetries of $3d$ orbitals and the complicated multiplet effects, the dichroic spectra show opposite signs for positive and negative crystal fields, but cannot be interchanged by simply reversing the sign with each other. Second, a clear spectral shift appears with tetragonal crystal field. The spectral shift to lower energies for $E \parallel c (E \perp c)$ corresponds to the lower of the d_{xy} (d_{xz}, d_{yz}) and d_{x2-y2} (d_{3z2-r2}) orbitals, and vice versa.

To provide the orbital occupations quantitatively, sum-rule analysis [45] is applied to the different linearly polarized absorption spectra of V $3d^1$ ($t_{2g}^1 e_g^0$). We define the electron polarization P following the equation used in $LaTiO_3$ with the same nominal $3d^1$ electronic configuration [46] and P can be expressed as

$$P = \frac{n_{xy} - n_{xz(yz)}}{n_{xy} + n_{xz(yz)}},$$

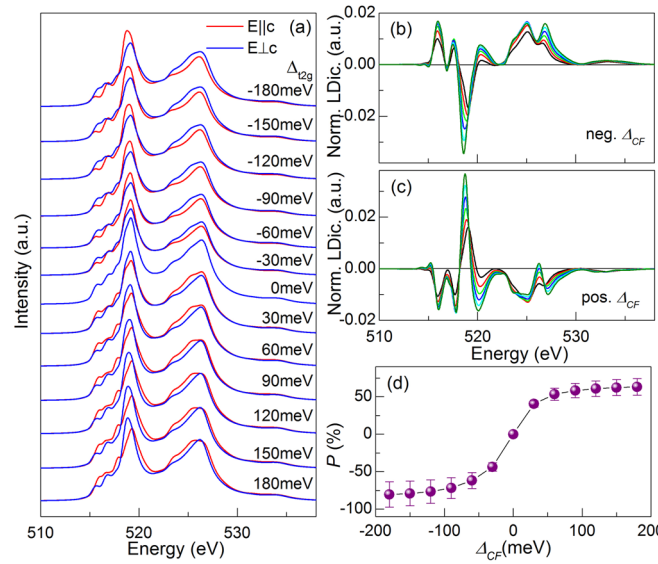

FIG. 5. (a) Calculated soft x-ray absorption spectra for a VO_6 $3d^1$ cluster with photon polarization parallel ($E \parallel c$) and perpendicular ($E \perp c$) to crystal c axis at different Δ_{t2g} and Δ_{eg} values. The Δ_{t2g} values are shown beside the corresponding plot. (b),(c) Normalized linear dichroic spectra, i.e. $(XAS_{E\perp c}\text{-}XAS_{E\parallel c})/[(2I_x + I_z)/3]$ for negative and positive Δ_{t2g}, Δ_{eg} values, respectively. (d) Calculated orbital polarization P vs Δ_{t2g}.

where n_{xy} and $n_{xz(yz)}$ denote the number of electrons in orbitals of xy and $xz(yz)$ symmetries. The P values are calculated by using the total number of electrons in t_{2g} states, i.e., $n_{t2g} = n_{xy} + n_{xz(yz)} = 1$, representing the d-p antibonding bands near the Fermi level [47,48]. Figure 5(d) represents the calculated orbital polarization P in the V t_{2g} states versus different crystal-field splitting values. The orbital polarizations in positive and negative crystal fields show opposite signs, representing the preferred electron occupation of respectively d_{xy} and $d_{xz(yz)}$ orbital level. Furthermore, a substantial orbital polarization P larger than 50% is obtained in response to a small crystal field, i.e., $\Delta_{t2g} = \pm 30$ meV, which we attribute to the insulating nature of the compound. The behavior is quite different from metallic $LaNiO_3$ thin films and heterostructures where a considerable bandwidth should be considered [47]. The strong sensitivity of orbital occupation to small tetragonal crystal-field strength further suggests that strain can suppress the orbital fluctuations in the system and can be used as an efficient mean to tailor electronic structures. The observed nearly complete orbital occupancy, i.e., more than 85% of the electrons showing d_{xy} orbital symmetry at $\Delta_{t2g} = 180$ meV with $P > 70\%$, indicates a strong electron correlation effect which shows consistency with the results suggested by LDA+DMFT calculation [14].

III. CONCLUSION

In summary, CI cluster calculations have been carried out to understand the multiplet structures and local ground-state properties of the orthorhombic distorted SVO compound. The good consistency of the spectral line shape between the simulated and experimental spectra suggests an appreciate

tetragonal crystal-field splitting, i.e., Δ_{t2g} not less than 180 meV, which supports the tetragonal crystal splitting scenario as the underlying mechanism for the MIT. Motivated by the synthesis difficulties in controlling the valence state of vanadium oxides and the importance of identifying the chemical valence in understanding the metal-insulator transition mechanism, we compare the V L_{23}-edge absorption spectra of vanadium oxides with similar VO_6 octahedral environment for formal d electrons from $3d^0$ to $3d^3$. All the simulated spectra show reasonable agreements with the experimental spectra. We further provide simulations for different cubic crystal-field splittings. A further comparison to a well-defined measured absorption spectrum can provide the actual crystal-field strength which is valuable for engineering of functional vanadium oxides. We finally show the absorption spectra with different linearly polarized lights at different tetragonal crystal-field values. The quantitative analysis of orbital polarizations indicates a nonlinear orbital-lattice coupling. The strong sensitivities of orbital occupation to small tetragonal crystal field suggests the efficiency of strain in tailoring the electronic properties, which sheds light on technical applications of SVO-based thin films and heterostructures. Our simulations show the powerful feature of CI cluster calculation using a regular PC and its potential in understanding the local ground-state properties.

ACKNOWLEDGMENTS

This project was funded by National Natural Science Foundation of China (Grant No. 11704317) and China Postdoctoral Science Foundation (Grant No. 2016M602064). We also acknowledge the support by the National Natural Science Foundation of China (Grant No. U1332105), and the Fundamental Research Funds for Central Universities (Grant No. 20720160020).

[1] M. Brahlek, L. Zhang, J. Lapano, H.-T. Zhang, R. Engel-Herbert, N. Shukla, S. Datta, H. Paik, and D. G. Schlom, MRS Commun. **7**, 27 (2017).
[2] J. A. Moyer, C. Eaton, and R. Engel-Herbert, Adv. Mater. **25**, 3578 (2013).
[3] L. Zhang, Y. Zhou, L. Guo, W. Zhao, A. Barnes, H.-T. Zhang, C. Eaton, Y. Zheng, M. Brahlek, H. F. Haneef *et al.*, Nat. Mater. **15**, 204 (2016).
[4] G. Kotliar, S. Y. Savrasov, K. Haule, V. S. Oudovenko, O. Parcollet, and C. A. Marianetti, Rev. Mod. Phys. **78**, 865 (2006).
[5] F. Lechermann, A. Georges, A. Poteryaev, S. Biermann, M. Posternak, A. Yamasaki, and O. K. Andersen, Phys. Rev. B **74**, 125120 (2006).
[6] J. M. Tomczak, M. Casula, T. Miyake, and S. Biermann, Phys. Rev. B **90**, 165138 (2014).
[7] A. Sekiyama, H. Fujiwara, S. Imada, S. Suga, H. Eisaki, S. I. Uchida, K. Takegahara, H. Harima, Y. Saitoh, I. A. Nekrasov *et al.*, Phys. Rev. Lett. **93**, 156402 (2004).
[8] M. Takizawa, M. Minohara, H. Kumigashira, D. Toyota, M. Oshima, H. Wadati, T. Yoshida, A. Fujimori, M. Lippmaa, M. Kawasaki *et al.*, Phys. Rev. B **80**, 235104 (2009).
[9] S. Aizaki, T. Yoshida, K. Yoshimatsu, M. Takizawa, M. Minohara, S. Ideta, A. Fujimori, K. Gupta, P. Mahadevan, K. Horiba *et al.*, Phys. Rev. Lett. **109**, 056401 (2012).
[10] K. Yoshimatsu, K. Horiba, H. Kumigashira, T. Yoshida, A. Fujimori, and M. Oshima, Science **333**, 319 (2011).
[11] K. Yoshimatsu, E. Sakai, M. Kobayashi, K. Horiba, T. Yoshida, A. Fujimori, M. Oshima, and H. Kumigashira, Phys. Rev. B **88**, 115308 (2013).
[12] M. Kobayashi, K. Yoshimatsu, E. Sakai, M. Kitamura, K. Horiba, A. Fujimori, and H. Kumigashira, Phys. Rev. Lett. **115**, 076801 (2015).
[13] M. Gu, S. Wolf, and J. Lu, Adv. Mater. Interfaces **1**, 1300126 (2013).
[14] Z. Zhong, M. Wallerberger, J. M. Tomczak, C. Taranto, N. Parragh, A. Toschi, G. Sangiovanni, and K. Held, Phys. Rev. Lett. **114**, 246401 (2015).
[15] A. Sharma, M. Varshney, W. Cheol Lim, H.-J. Shin, J. Pal Singh, S. Ok Won, and K. Hwa Chae, Phys. Chem. Chem. Phys. **19**, 6397 (2017).
[16] M. Demeter, M. Neumann, and W. Reichelt, Surf. Sci. **454–456**, 41 (2000).
[17] S. Lee, T. Meyer, S. Park, T. Egami, and H. Lee, Appl. Phys. Lett. **105**, 223515 (2014).
[18] W. Liang, M. Gao, C. Lu, Z. Zhang, C. Chan, L. Zhuge, J. Dai, H. Yang, C. Chen, B. Park *et al.*, ACS Appl. Mater. Interfaces **10**, 8341 (2018).
[19] M. Imada, A. Fujimori, and Y. Tokura, Rev. Mod. Phys. **70**, 1039 (1998).
[20] E. Nazarenko, J. E. Lorenzo, Y. Joly, J. L. Hodeau, D. Mannix, and C. Marin, Phys. Rev. Lett. **97**, 056403 (2006).
[21] S. Anissimova, D. Parshall, G. Gu, K. Marty, M. Lumsden, S. Chi, J. Fernandez-Baca, D. Abernathy, D. Lamago, J. Tranquada *et al.*, Nat. Commun. **5**, 3467 (2014).
[22] H. Sawa, E. Ninomiya, T. Ohama, H. Nakao, K. Ohwada, Y. Murakami, Y. Fujii, Y. Noda, M. Isobe, and Y. Ueda, J. Phys. Soc. Jpn. **71**, 385 (2002).
[23] T. Yoshino, M. Okawa, T. Kajita, S. Dash, R. Shimoyama, K. Takahashi, Y. Takahashi, R. Takayanagi, T. Saitoh, D. Ootsuki *et al.*, Phys. Rev. B **95**, 075151 (2017).
[24] M. W. Haverkort, Z. Hu, A. Tanaka, W. Reichelt, S. V. Streltsov, M. A. Korotin, V. I. Anisimov, H. H. Hsieh, H.-J. Lin, C. T. Chen *et al.*, Phys. Rev. Lett. **95**, 196404 (2005).
[25] R. J. O. Mossanek, M. Abbate, T. Yoshida, A. Fujimori, Y. Yoshida, N. Shirakawa, H. Eisaki, S. Kohno, P. T. Fonseca, and F. C. Vicentin, Phys. Rev. B **79**, 033104 (2009).
[26] M. Wu, H. Xin, J. Wang, X. J. Li, X. B. Yuan, H. Zeng, J.-C. Zheng, and H.-Q. Wang, J. Synchrotron Radiat. **25**, 777 (2018).
[27] J.-H. Park, L. H. Tjeng, A. Tanaka, J. W. Allen, C. T. Chen, P. Metcalf, J. M. Honig, F. M. F. de Groot, and G. A. Sawatzky, Phys. Rev. B **61**, 11506 (2000).
[28] E. Benckiser, L. Fels, G. Ghiringhelli, M. Moretti Sala, T. Schmitt, J. Schlappa, V. N. Strocov, N. Mufti, G. R. Blake, A. A. Nugroho *et al.*, Phys. Rev. B **88**, 205115 (2013).
[29] D. Maganas, M. Roemelt, M. Havecker, A. Trunschke, A. Knop-Gericke, R. Schlogl, and F. Neese, Phys. Chem. Chem. Phys. **15**, 7260 (2013).
[30] C. Hébert, M. Willinger, D. Su, P. Pongratz, P. Schattschneider, and R. Schlögl, Eur. Phys. J. B **28**, 407 (2002).

[31] M. Zhuang, W. Zhang, and N. Ming, Phys. Rev. B **57**, 10705 (1998).
[32] J. A. Aramburu, P. Garcia-Fernandez, J. M. García-Lastra, M. T. Barriuso, and M. Moreno, Phys. Rev. B **85**, 245118 (2012).
[33] F. M. F. de Groot, J. C. Fuggle, B. T. Thole, and G. A. Sawatzky, Phys. Rev. B **42**, 5459 (1990).
[34] A. Tanaka and T. Jo, J. Phys. Soc. Jpn. **63**, 2788 (1994).
[35] S. P. Cramer, F. M. F. DeGroot, Y. Ma, C. T. Chen, F. Sette, C. A. Kipke, D. M. Eichhorn, M. K. Chan, W. H. Armstrong, E. Libby *et al.*, J. Am. Chem. Soc. **113**, 7937 (1991).
[36] B. P. von der Heyden, A. N. Roychoudhury, T. Tyliszczak, and S. C. B. Myneni, Am. Mineral. **102**, 674 (2017).
[37] A. E. Bocquet, T. Mizokawa, K. Morikawa, A. Fujimori, S. R. Barman, K. Maiti, D. D. Sarma, Y. Tokura, and M. Onoda, Phys. Rev. B **53**, 1161 (1996).
[38] T. Saitoh, A. E. Bocquet, T. Mizokawa, and A. Fujimori, Phys. Rev. B **52**, 7934 (1995).
[39] J. H. Haeni, P. Irvin, W. Chang, R. Uecker, P. Reiche, Y. L. Li, S. Choudhury, W. Tian, M. E. Hawley, B. Craigo *et al.*, Nature (London) **430**, 758 (2004).
[40] D. G. Schlom, L.-Q. Chen, C.-B. Eom, K. M. Rabe, S. K. Streiffer, and J.-M. Triscone, Annu. Rev. Mater. Res. **37**, 589 (2007).
[41] S. He, J. He, W. Zhang, L. Zhao, D. Liu, X. Liu, D. Mou, Y.-B. Ou, Q.-Y. Wang, Z. Li *et al.*, Nat. Mater. **12**, 605 (2013).
[42] L. Howald, E. Stilp, F. Baiutti, C. Dietl, F. Wrobel, G. Logvenov, T. Prokscha, Z. Salman, N. Wooding, D. Pavuna *et al.*, Phys. Rev. B **97**, 094514 (2018).
[43] V. Moshnyaga, B. Damaschke, O. Shapoval, A. Belenchuk, J. Faupel, O. I. Lebedev, J. Verbeeck, G. van Tendeloo, M. Mücksch, V. Tsurkan *et al.*, Nat. Mater. **2**, 247 (2003).
[44] W. S. Choi, J.-H. Kwon, H. Jeen, J. Hamann-Borrero, A. Radi, S. Macke, R. Sutarto, F. He, G. A. Sawatzky, V. Hinkov *et al.*, Nano Lett. **12**, 4966 (2012).
[45] G. van der Laan, J. Phys. Soc. Jpn. **63**, 2393 (1994).
[46] M. Wu, J.-C. Zheng, and H.-Q. Wang, J. Appl. Crystallogr. **50**, 576 (2017).
[47] M. Wu, E. Benckiser, M. W. Haverkort, A. Frano, Y. Lu, U. Nwankwo, S. Brück, P. Audehm, E. Goering, S. Macke *et al.*, Phys. Rev. B **88**, 125124 (2013).
[48] O. E. Peil, M. Ferrero, and A. Georges, Phys. Rev. B **90**, 045128 (2014).